Deep Neural Networks for Skin Cancer Classification: Analysis of Melanoma Cancer Data

Stephen Afrifa [1,2,*], Vijayakumar Varadarajan [3,4,5,*], Peter Appiahene [2], Tao Zhang [1], Daniel Gyamfi [6], and Rose-Mary Owusuaa Mensah Gyening [7]

[1] Department of Information and Communication Engineering, Tianjin University, Tianjin, China
[2] Department of Information Technology and Decision Sciences, University of Energy and Natural Resources, Sunyani, Ghana
[3] Research Division, Swiss School of Business and Management, Geneva, Switzerland
[4] International Divisions, Ajeenkya D. Y. Patil University, Pune, India
[5] Department of Computer Science and Information Technology, La Trobe University, Sydney, Australia
[6] Department of Computer Science and Mathematics, Saint Louis University, Missouri, United States of America
[7] Department of Computer Science, Kwame Nkrumah University of Science and Technology, Kumasi, Ghana
Email: afrifastephen@tju.edu.cn (S.A.); vijayakumar.varadarajan@gmail.com (V.V.); peter.appiahene@uenr.edu.gh (P.A.); zhangtao@tju.edu.cn (T.Z.); daniel.gyamfi@slu.edu (D.G.); rmo.mensah@knust.edu.gh (R.-M.O.M.G.)
*Corresponding author

***Abstract*—The skin is the largest organ in the human body, serving as its outermost covering. The skin protects the human body from elements and viruses, regulates temperature, and provides cold, heat, and touch sensations. A skin lesion is a type of abnormality in or on the skin. Melanoma skin cancer is the most deadly and deadliest of the skin cancer family. Several researchers have developed non-invasive approaches for detecting skin cancer as technology has advanced. The early detection of a skin lesion is crucial for its treatment. In this study, we introduce a deep neural network for diagnosing skin melanoma in its early stages using Convolutional Neural Network (CNN), Capsule Neural Network (CapsNet), and Gabor Capsule Neural Network (GCN). To train the models, the International Skin Imaging Collaboration (ISIC) melanoma data is used. Prior to deploying deep neural networks, methods such as preprocessing dataset images to remove noise and lighting concerns for better visual information are used. Deep Learning (DL) models are employed to classify the images' melanoma lesions. The performance of the proposed approaches is evaluated using cutting-edge performance metrics, and the results show that the presented method beats state-of-the-art techniques. The models achieve an average accuracy of 90.30% for CNN, 87.90% for CapsNet, and 86.80% for GCN, demonstrating their capability to recognize and segment skin lesions. These developments enable health practitioners to provide more accurate diagnoses and help government healthcare systems with early identification and treatment initiatives.**

***Keywords*—deep learning, capsule network, melanoma, skin cancer, neural networks**

I. Introduction

Skin is the biggest organ in the human body and the body's outer layer [1]. The skin protects the human body from elements and microorganisms entering the body, aids in temperature regulation, and allows for the sensations of cold, heat, and touch [2]. A skin lesion arises when a piece of the skin is abnormal in relation to other parts of the skin. Skin lesions are caused by infections that occur in or on the skin [3]. Melanoma is the worst of the malignant disorders that affect the skin. Melanoma is the least common type of skin cancer, yet it is the deadliest. Melanoma can spread to other regions of the body and is caused by malignant transformation of melanocytes produced from neural crest neoplasia [4]. According to the World Health Organization (WHO), the prevalence of both non-melanoma and melanoma skin cancers has increased in recent decades. Each year, between 2 and 3 million non-melanoma skin cancers and 132,000 melanoma skin cancers are diagnosed worldwide [5]. According to Skin Cancer Foundation Statistics, one in every three malignancies diagnosed is skin cancer, and one in every five Americans will acquire skin cancer throughout their lifetime [6].

Skin cancer detection is challenging, and even experienced expert dermatologists had a 60% success rate until the advent of dermoscopic pictures, which boosted success to 75% to 84% [7]. The problem is that malignant lesions are frequently quite similar to benign moles, and both have tiny diameters that do not allow for decent images with standard cameras. Melanoma and nevus, for example, are both melanotic kinds, and as a result, the categorization difficulties between them are considerably

Manuscript received May 31, 2024; revised June 24, 2024; accepted July 10, 2024; published January 9, 2025.

greater [8]. The most important aspect of treating skin cancer is detecting it early and accurately. For example, if melanoma is not detected in its early stages, it begins to develop and spreads over the outer skin layer, eventually infiltrating the deep layers and connecting with the blood and lymph arteries [9, 10]. Several individuals have turned to Compute-Aided Diagnosis (CAD) to diagnose skin cancer since the introduction of technology. The combination of Artificial Intelligence (AI) and non-invasive skin imaging offers up a wide range of possibilities since AI can execute jobs that humans cannot do in a fair period of time. To identify skin cancer, several researchers have used Machine Learning (ML), as well as Deep Learning (DL) methods.

For example, Grignaffini *et al*. [11] created a melanoma detection task that was performed with the help of a Convolutional Neural Network (CNN) and the handcrafted texture features of the dermoscopic images as additional input in the training phase. They attempted to determine if the dermoscopic image preparation and segmentation procedures might be skipped while retaining good classification performance. However, their research was hampered by the unbalanced nature of medical imagery. In another related study, Ichim *et al*. [12] introduced two neural network ensembles for the identification of four skin lesions, based on the fusing of the choices of the component neural networks. All models' individual F1 scores for each class and the global system varied from 81.36% to 94.17%. Furthermore, Juan *et al*. [13] has presented SkinFLNet, a revolutionary skin cancer classification approach that makes use of model fusion and lifetime learning technology. The SkinFLNet's deep convolutional neural networks were trained on a dataset of 1,215 clinical pictures of skin malignancies diagnosed at Taichung and Taipei Veterans General Hospitals from 2015 to 2020. Their research discovered an effective skin cancer classification system that can be trained on a relatively short dataset with an accuracy of 85% utilizing model fusion and lifetime learning methods. As previously stated, the use of CAD in the identification of skin cancer has been successful, for instance, (Fawzy *et al*. [14] proposed a Computer-Aided Diagnostic (CAD) system. Their experimental findings demonstrated that the proposed method enabled classification accuracy. Their proposed solution provides a less complex and cutting-edge framework for automating skin cancer detection and accelerating the diagnosis procedure in order to save a life. It has been observed that, Riyadh *et al*. [15] demonstrated a unique convolutional neural network-based technique for identifying skin cancer in clinical skin pictures. Their experiments revealed that the strategy has a high level of categorization accuracy.

Many studies have been undertaken on the effectiveness of using CNN to categorize skin cancer lesion [16]. Although, data imbalance has been a challenging factor in medical diagnosis, this study seeks to address the limitations of existing approaches by offering a unique method for detecting melanoma lesions on the skin using a deep neural network technology, namely Convolutional Neural Network (CNN), Capsule Neural Network (CapsNet), and Gabor Capsule Network (GCN). The goal is to advance the model's performance by preparing the dataset and providing an acceptable technique for dealing with imbalanced datasets and missing values. The major contributions of the study are as follows:

1) The study utilizes deep learning models of the CNN, CapsNet, and GCN to categorize melanoma lesions.
2) The study also employs a novel strategy to detecting class imbalance by developing a cutting-edge method for achieving higher loss values in terms of entropy loss.
3) The efficacy of deep learning models is assessed utilizing cross validation approaches and cutting-edge performance evaluation criteria.
4) The study highlights the most current use of DL in the analysis and classification of melanoma lesions.

The remainder of the paper is arranged as follows. Section II outlines the methodologies utilized in this study, which include a thorough evaluation of the data, preparation processes, and deep learning models. Section III also includes an overview of the experimental outcomes. Section IV includes a detailed description of the study in the Discussion section. Section V addresses the study's conclusion and shortcomings.

II. Materials and Methods

This segment outlines the techniques used in this study. It covers everything from data collection to the models deployed and the metrics used to evaluate their effectiveness. The strategies are fully addressed in the subsections that follow.

A. Data Collection

The study utilized the publicly available dataset from the International Skin Imaging Collaboration (ISIC) platform [17] accessed on November 22, 2023. The dataset contains 18,133 images from 2,463 patients with a total of 7,369 number of lesions. The dataset is binary with benign and malignant categories. The total dataset is exposed to the training techniques of the study.

B. Proposed Framework of the Study

The paradigm for categorizing skin cancer employed in this investigation is depicted in Fig. 1. Image augmentation, grayscale conversion, de-noising approach, Contrast Limited Adaptive Histogram Equalization (CLACHE), and feature extraction techniques were used to the dataset. The preparation procedures outlined above are utilized to generate clean data that the suggested models can interpret during training. For classifying skin cancer masses, the proposed deep learning models used in this study include CNN, CapsNet, and GCN. Preprocessed data was divided into three categories: training, validation, and testing. The research was divided into two parts: training (80%) and testing (20%). A subset of the testing set (20%) was used to validate the deep learning models. Deep learning model training outcomes are evaluated using a variety of performance assessment criteria.

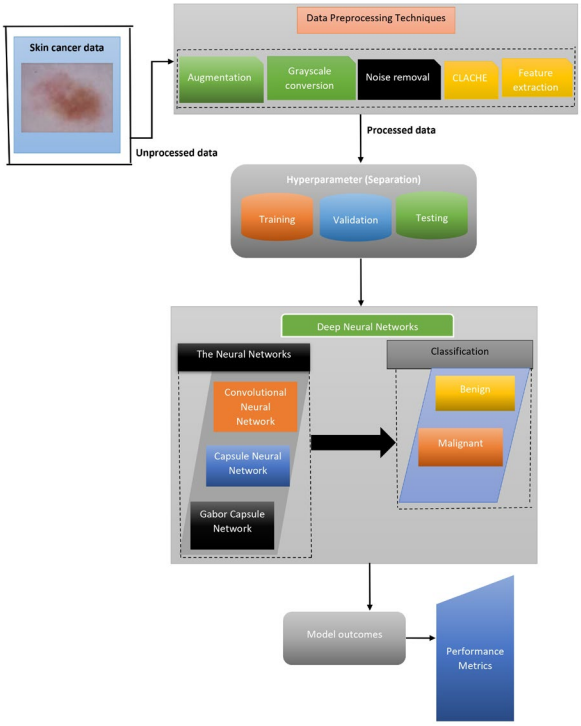

Fig. 1. Proposed framework of the study.

C. Data Preprocessing Techniques

Data preparation is critical in Deep Learning (DL) analysis since it allows the models to be trained. Data preparation improves the quality, reliability, and efficacy of modeling approaches, making the data more suited for increasing deep learning model comprehension and performance [18]. The sections that follow describe the various methodologies employed in the current study.

1) Data augmentataion technique: Data augmentation is a technique that artificially increases the training set by making modified copies of existing data. Data augmentation increases the performance and results of machine learning models by creating fresh and unique examples for training datasets [19]. When the dataset is huge and diversified, deep learning models perform well. Rotation and rescaling methods are employed in augmentation operations. The photos are loaded and enhanced in Keras version 2.13 (Google LLC, Mountain View, California, United States) using the Image Data Generator class. These strategies were used to enhance model prediction accuracy by adding more training data into models and avoiding data shortages. The Image Data Generator class properties and associated settings are shown in Table I.

TABLE I. IMAGE DATA GENERATOR CLASS PARAMETERS

Setting	Value
Rotation	10°
Width shift	2 pixels
Height shift	22 pixels
Shear	0.2 radians
Rescale	[0, 255] to [0, 1]
Fill mode	Nearest

2) Grayscale conversion technique: The RGB values of Red (R), Green (G), and Blue (B) are converted to grayscale for each picture. A grayscale picture is one composed of several shades of gray (or black and white). Grayscale images have the potential to reduce the computational cost of image processing activities. This is due to the reduction of the number of channels from three (RGB) to one (gray). The luminosity method was used to convert grayscale to black and white. The luminosity method is expressed in Eq. (1).

$$Y = 0.299R + 0.587G + 0.114B \quad (1)$$

Grayscale conversion helps to simplify algorithms and eliminate difficulties related to processing demands.

3) Noise resuction technique: Bilateral filtering is used to minimize noise in pictures. Bilateral filtering is a method of smoothing images while retaining their edges. Bilateral filtering is a form of non-local denoising. Non-Local Means (NLM) denoising is a method of reducing noise from a photograph while preserving its edges and characteristics [20]. It compares each pixel in the image to all of the others, calculating their similarity and using that information to estimate the value of the noisy pixel [21]. Even if they are not in the same place, comparable patches in an image have comparable values for any NLM denoising algorithm. The algorithm can forecast the image's structure and reduce noise without blurring or distorting the edges or features by comparing all patches to each other. The numerical representation of bilateral filtering is shown in Eq. (2).

$$BF[I]_p = \frac{1}{W_p}\sum_{q\in S}\left[\left(G_{\sigma s}(||p-q||)\right)\cdot(G_{\sigma r}(|I_p - I_q|))\right]\cdot I_q \quad (2)$$

where $BF[I]_p$ is the yield of bilateral filtering at pixel p, I_q is the intensity at pixel q, $\frac{1}{W_p}$ is the normalization factor, W_p is the normalization term, $G_{\sigma s}$ is the Gaussian function for the standard deviation of spatial Gaussian component, $||p-q||$ is the Euclidean distance between p and q, and $G_{\sigma r}$ is the Gaussian function for the standard deviation of the range Gaussian component, additionally, I_p is the absolute intensity value at p, and I_q is the absolute intensity value at q.

4) Contrast limited adaptive histogram equalization technique: To enhance the contrast of each picture, the Contrast Limited Adaptive Histogram Equalization (CLAHE) approach is used. CLAHE is a technique for boosting visual contrast by spreading the intensity values in a picture, which is especially useful in low contrast images. The CLAHE algorithm defined in the createCLAHE and OPENCV routines is used to process the normalized and denoised grayscale image. The CLAHE-enhanced image is then converted back to RGB format.

5) Feature extraction technique: The labels are stored in separate lists, while the features are concatenated into a single array. The feature array has been rearranged in four

dimensions. The feature array is then normalized using the StandardScaler function from Scikit-learn [22]. The normalized features and labels are divided into training, validation, and testing sets using the K-fold cross-validation method. The K-Fold object folds data 10 times. For each fold, the training data is divided into two sets: 80% training and 20% validation. To avoid network overfitting, K-fold cross-validation is employed. Cross-validation reduces overfitting by providing an estimate of the model's performance on unseen data [23]. The validation sets are intended to be used to track a model's performance throughout training.

D. Deep Neural Networks

This section goes into great detail about each model and its design. Convolutional Neural Networks (CNN), Capsule Neural Networks (CapsNet), and Gabor Capsule Networks (GCN) are the deep neural networks used in this study. The GCN utilizes a capsule network design, with the first layer being a convolutional Gabor layer.

1) Convolutional neural network: A CNN is a deep learning system that can take an input image, prioritize different aspects/objects in the image (via learnable weights and biases), and differentiate one from the other [24]. The CNN was used to classify the melanoma lesion in the current study. The CNN employs the VGG16 architecture of the Visual Geometry Group Network (VGGNet). The CNN's architecture incorporates convolutional and max-pooling layers. The SoftMax activation function was used, with a regularization factor of 0.0001 and a maximum iteration of 10. SoftMax is a CNN activation function frequently used in the output layer.

In the sequential model, the CNN made use of convolutional and max-pooling layers. After the convolutional layers were finished, the data was flattened to generate three entirely linked layers for output using the SoftMax activation function. The total number of trainable parameters is 979,330, with a sampling of the total based on VGG16 pre-trained values. The CNN used in this work consists of two convolutional layers, two max pooling layers, two dropout layers, a flatten layer, and two fully linked layers. The two dropouts are important tools for improving CNN performance and generalization because they reduce overfitting, promote robust feature learning, and handle big and complex models fast. The first dropout reduces noise in the feature maps, while the second controls the entire CNN architecture for improved output. In addition, the flattened layer converts the spatially ordered feature maps into a one-dimensional vector that fully linked layers can use to produce predictions. The network's architecture requires this flattened representation to connect convolutional layers to fully connected layers. Finally, the pictures are classed by the entirely linked layers, which allows the melanoma lesion to be identified. The fully connected layer makes final predictions using the hierarchical features learnt by the convolutional and pooling layers. Table II provides an overview of the layers employed in the CNN design.

TABLE II. ARCHITECTURAL OUTLINE OF THE CNN

Layer (type)	Output Shape	Param #
Block1_Conv1 (Conv2D)	(None, 126, 126, 64)	1792
Block1_Pool (MaxPooling2D)	(None, 63, 63, 64)	0
Block2_Conv1 (Conv2D)	(None, 61, 61, 128)	73856
Block2_Pool (MaxPooling2D)	(None, 30, 30, 128)	0
Block3_Conv1 (Conv2D)	(None, 28, 28, 256)	295168
Block3_Pool (MaxPooling2D)	(None, 14, 14, 256)	0
Block4_Conv1 (Conv2D)	(None, 12, 12, 256)	590080
Block4_Pool (MaxPooling2D)	(None, 6, 6, 256)	0
Block4_Dropout (Dropout)	(None, 6, 6, 256)	0
Flatten (Flatten)	(None, 9216)	0
Dropout (Dropout)	(None, 9216)	0
Output (Dense)	(None, 2)	18434
Total params	979330 (3.74 MB)	
Trainable params:	979330 (3.74 MB)	
Non-trainable params:	0 (0.00 Byte)	

2) Capsule network: The CapsNet design consists of two convolutional layers, a primary capsule block and a class capsule block. A capsule network is a group of neurons in which the activity vector represents the instantiation parameters and the length of the vector signifies the likelihood of an entity's existence [25]. Capsule networks can learn image attributes such as deformations, position, and texture thanks to this feature. The three most common methods for creating capsules are auto-encoders, vector capsules based on dynamic routing, and matrix capsules based on Expectation-Maximization (EM) routing. This study's data was trained using vector capsules based on dynamic routing. Vector routings are used to express visual parameters in vector capsules. ReLU, Sigmoid, and Tangent functions are used as activation functions in CNNs [14]. As indicated in Eq. (3), the activation function for a vector capsule is known as a squash function.

$$v_j = \frac{\|s_j\|^2}{1+\|s_j\|^2} \frac{s_j}{\|s_j\|} \tag{3}$$

where v_j= output of capsule j, and s_j = entire input of the capsule. The entire input value of capsule s_j is found by the weighted sum of the forecast vectors ($U_{i|j}$) in lower-layered capsules excluding in the first layer of the capsule network. The forecast vector is formed by multiplying the output u_j of a capsule in the lower layer by a weight matrix presented in Eqs. (4) and (5).

$$s_j = \sum_i c_{ij} u_{i|j} \tag{4}$$

$$u_{i|j} = W_{ij} u_i \tag{5}$$

where c_{ij} = coupling coefficients that are resolute by the iterative lively routing process (Fig. 1). The coupling coefficients are determined by a SoftMax function which is expressed in Eq. (6).

$$c_{ij} = \frac{exp\,(a_{ij})}{\sum_k exp\,(a_{ik})} \tag{6}$$

where a_{ij}= log prior probability. In capsule networks, a margin loss has been proposed to determine the presence of objects of a particular class [26]. This margin loss is calculated as presented in Eq. (7).

$$L_k = T_k \max(0, m^+ - \| v_k \|^2)^2 + \lambda(1 - T_k) \max(0, \| v_k \| - m^-)^2 \quad (7)$$

The CNN's block 4 dropout layer's feature maps are delivered to the first convolutional layer (Block5_Conv1). The convolutional technique is used to build 7×7 feature maps, using 128 filters, a kernel size of 7×7, and ReLU activation. The second convolutional layer uses a convolution of 128 filters, a 6×6 kernel size, and ReLU activation to create 2×2 feature maps. The main capsule block is made up of a convolutional layer and a reshape layer. The contour layer generates 32-channeled 1×1 feature maps, which are then molded and compressed into two 16-dimensional capsules. The output of the main capsule layer is then sent to the Class capsule layer. The Class capsule's output is delivered to the last tier, the lambda layer. As the output layer, this layer computes the class probabilities. Table III depicts the capsule neural network architecture.

TABLE III. ARCHITECTURAL OUTLINE OF THE CAPSNET

Layer (type)	Output Shape	Param #
Block1_Conv1_input (InputLayer)	[(None, 128, 128, 3)]	0
Block1_Conv1 (Conv2D)	(None, 126, 126, 64)	1792
Block1_Conv2 (Conv2D)	(None, 124, 124, 64)	36928
Block1_Pool (MaxPooling2D)	(None, 62, 62, 64)	0
Block2_Conv1 (Conv2D)	(None, 60, 60, 128)	73856
Block2_Conv2 (Conv2D)	(None, 58, 58, 128)	147584
Block2_Pool (MaxPooling2D)	(None, 29, 29, 128)	0
Block3_Conv1 (Conv2D)	(None, 27, 27, 256)	295168
Block3_Conv2 (Conv2D)	(None, 25, 25, 256)	590080
Block3_Pool (MaxPooling2D)	(None, 12, 12, 256)	0
Block4_Conv1 (Conv2D)	(None, 10, 10, 256)	590080
Block4_Pool (MaxPooling2D)	(None, 5, 5, 256)	0
Block4_Dropout (Dropout)	(None, 5, 5, 256)	0
Block5_Conv1 (Conv2D)	(None, 4, 4, 128)	131200
Block5_Conv2 (Conv2D)	(None, 3, 3, 128)	65664
primarycap_conv2d (Conv2D)	(None, 1, 1, 32)	16416
primarycap_reshape (Reshape)	(None, 2, 16)	0
primarycap_squash (Lambda)	(None, 2, 16)	0
class__capsule_2 (Class_Capsule)	(None, 2, 16)	1024
lambda_2 (Lambda)	(None, 2)	0
Total params:	1949792 (7.44 MB)	
Trainable params:	1949792 (7.44 MB)	
Non-trainable params:	0 (0.00 Byte)	

3) Gabor capsule network: The architecture of the Gabor Capsule Network (GCN) is similar to that of the capsule network paradigm. The GCN architecture is made up of a convolutional block, a key capsule block, and a class capsule block. In image processing, a Gabor filter is a linear filter built by combining sinusoid and Gaussian functions [27]. The Gabor filter may be customized by changing its orientation, scale, aspect ratio, frequency, and phase. Eq. (8) can be used to express a Gabor filter numerically.

$$g\lambda, \theta, \sigma, \gamma(x, y) = exp\left(-\frac{x'+\gamma y'^2}{2\sigma^2}\right) cos(2\pi \frac{x'}{\lambda} + \phi) \quad (8)$$

where $x' = x \cos\theta + y \sin\theta$, $y' = -x \sin\theta + y \cos\theta$. Gabor filters are powerful tools that may be used to recognize edges, analyze texture, and extract characteristics from pictures. Gabor filters may be used to extract features for use in CNNs as preprocessing approaches. In the convolution process, a group of global Gabor filters is utilized to extract properties from an input image. This convolution operation (*) applied to the image and the global Gabor filter bank $G(x, y: w, \theta)$, generates a set of features ($O_{m,\ n}(x,\ y)$) that can be represented mathematically by the Eq. (9):

$$Om, n(x, y) = I(x, y) * G(x, y: w, \theta) \quad (9)$$

The Gabor capsule network (GCN) architecture is shown in Table IV. The CNN's block 4 dropout layer's feature maps are sent into the first convolutional layer (Block5_Conv1). The convolutional technique is used to build 7×7 feature maps, using 128 filters, a kernel size of 7×7, and ReLU activation. The second convolutional layer then generates 7×7 feature maps using 256 Gabor filters, a 7×7 kernel size, and ReLU activation. The primary capsule block consists of a convolutional layer and a reshape layer. The convoluted layer generates 32-channel 3×3 feature maps, which are then molded and compressed into 18 capsules with 16 filters. The output from the main capsule layer is sent to the Class capsule layer. The Class capsule's output is flattened and sent to the lambda layer. This layer is the output layer, which computes the class probabilities.

TABLE IV. ARCHITECTURAL OUTLINE OF THE GCN

Layer (type)	Output Shape	Param #
Block1_Conv1_input (InputLayer)	[(None, 128, 128, 3)]	0
Block1_Conv1 (Conv2D)	(None, 126, 126, 64)	1792
Block1_Conv2 (Conv2D)	(None, 124, 124, 64)	36928
Block1_Pool (MaxPooling2D)	(None, 62, 62, 64)	0
Block2_Conv1 (Conv2D)	(None, 60, 60, 128)	73856
Block2_Conv2 (Conv2D)	(None, 58, 58, 128)	147584
Block2_Pool (MaxPooling2D)	(None, 29, 29, 128)	0
Block3_Conv1 (Conv2D)	(None, 27, 27, 256)	295168
Block3_Conv2 (Conv2D)	(None, 25, 25, 256)	590080
Block3_Pool (MaxPooling2D)	(None, 12, 12, 256)	0
Block4_Conv1 (Conv2D)	(None, 10, 10, 256)	590080
Block4_Pool (MaxPooling2D)	(None, 5, 5, 256)	0
Block4_Dropout (Dropout)	(None, 5, 5, 256)	0
Block5_Conv1 (Conv2D)	(None, 4, 4, 128)	131200
GaborLayer (GaborLayer)	(None, 2, 2, 128)	0
primarycap_conv2d (Conv2D)	(None, 1, 1, 32)	16416
primarycap_reshape (Reshape)	(None, 2, 16)	0
primarycap_squash (Lambda)	(None, 2, 16)	0
class__capsule_3 (Class_Capsule)	(None, 2, 16)	512
lambda_3 (Lambda)	(None, 2)	0
Total params:	1883616 (7.19 MB)	
Trainable params:	1883616 (7.19 MB)	
Non-trainable params:	0 (0.00 Byte)	

E. Performance Evaluation Metrics

Model evaluation is critical since it evaluates a model's performance as a generic model. A performance evaluation is used to test the generalization accuracy of a

model using unseen/out-of-sample data [28]. The models were evaluated using performance assessment criteria such as accuracy, loss, precision, recall, specificity, and Receiver Operating Characteristic Area under the Curve (ROCAUC). True Positives (TP), False Negatives (FN), False Positives (FP), and True Negatives (TN) are some of the measures assessed.

The number of correctly classified instances is divided by the total number of occurrences in the dataset to measure accuracy. Eq. (10) represents accuracy.

$$Accuracy = \frac{TP+TN}{TP+TN+FP+FN} \quad (10)$$

Loss in a machine learning model evaluates the inaccuracy or disparity between predicted and real data. In neural networks, the most commonly used loss function is cross-entropy. The loss function is represented by Eq. (11).

$$loss = \sum_{i=1}^{n}\sum_{j=1}^{m} y_{i,j}\, log(p_i, j) \quad (11)$$

where n = number of samples, y = true label or ground truth, m = number of classes, j = class iterator, i = samples iterator and p = predicted probability or score.

Precision assesses a model's ability to accurately detect positive examples among all predicted instances. It assesses the precision of a model's positive predictions. Recall (Sensitivity) measures a model's ability to correctly identify all positive occurrences in a dataset [29]. The capacity of a model to correctly detect negative cases among all negative examples in a dataset is measured by specificity. It assesses the precision of a model's positive predictions. Another term for it is the True Negative Rate (TNR). The ROC curve is used to show sensitivity vs the false positive rate (1-specificity) at different thresholds. In other words, the ROC curve indicates the performance of a classification model. A threshold is a number that determines how the prediction of a model is classed.

The False Positive Rate (FPR) is the proportion of false positive events anticipated as positive by a model out of all genuine negative cases. The Area under the Curve (AUC) score assesses the model's overall performance by calculating the area under the ROC curve.

Eq. (12) is used to determine precision, whereas Eq. (13) may be used to calculate recall. Eq. (14) defines specificity, while Eqs. (15)–(17) reveal the formula that makes up the ROC.

$$Precision = \frac{TP}{TP+FP} \quad (12)$$

$$Recall = \frac{TP}{TP+FN} \quad (13)$$

$$Specificity = \frac{TN}{TN+FP} \quad (14)$$

$$\text{FPR} = 1 - \text{Specificity} \quad (15)$$

$$FPR = 1 - \frac{TN}{TN+FP} \quad (16)$$

$$FPR = \frac{FP}{FP+TN} \quad (17)$$

III. Experimental Results

This section presents the experimental configuration setups and the results obtained by the deep neural network models employed in this study.

A. Working Environment and Experimental Setup Configurations

As a consequence, the deep learning models were trained using the Google Colab platform with Python version 3.11.4 (The Python Software Foundation (PSF), 1209 Orange Street, Wilmington, Delaware, USA). The installed Random Access Memory (RAM) capacity is 12.0 gigabytes (GB), and the operating system is 64-bit. Table V displays the system characteristics and experimental settings used to get the results. The experimental system is composed of five nodes, each having an Intel(R) Core(TM) i5-1155G7 @ 2.50GHz, eight cores, and twelve gigabytes of RAM.

TABLE V. Working Environment and Specifications

Product	Specification
Processor	11th Gen Intel(R) Core(TM) i5-1155G7 @2.50Ghz 2.50GHz
RAM	12.0 GB
System	64-bit operating system

The experimental formation used to acquire the training data is summarized in Table VI. With data volumes ranging from 5 GB to 15 GB, the deep learning models, thus, CNN, CapsNet, and GCN were created and evaluated. Each application is run by a windows bash script for each parameter values.

TABLE VI. System Configuration and Setups

Configuration parameter	Minimum value	Maximum value
Number of executors (-num-executor)	2	10
Number of cores per Executor (-executor-cores)	1	8
Executor memory (-executor-memory)	1	12
Data capacity	1 GB	15 GB

B. Performance of the Deep Learning Models

The performance of the DL models on the melanoma dataset is presented in this section. The subsections that follow provide in-depth examination of the results

1) Skin cancer data interpretability: The Class Activation Mapping (CAM) approach was used to identify the elements of an image that influence the judgment or classification of a DL model. CAMs help to explain the classifications or predictions of a deep learning model. This ensures that each model predicts using the relevant picture parts in each class. During this study, the models are tested and assessed using Gradient-weighted Class Activation Mapping (Grad-CAM). Using the gradients of the final convolutional layer, Grad-CAM generates a weighted mixture of feature maps. Figs. 2 and 3 depict the

Grad-CAM of each deep learning model on benign and malignant images, respectively.

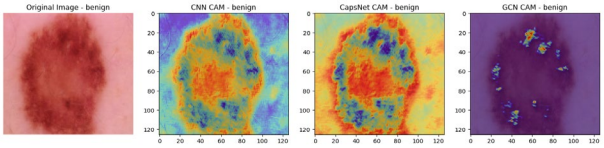

Fig. 2. Grad-CAM of the models on the benign image.

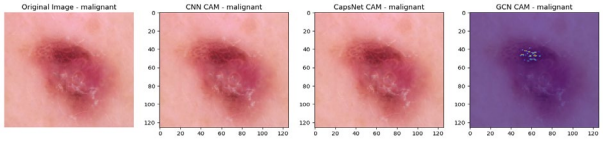

Fig. 3. Grad-CAM of the models on the malignant image.

2) Evaluation of the models on the skin cancer data: This study applied the Convolutional Neural Network (CNN), Capsule Neural Network (CapsNet), and Gabor Capsule Network (GCN) on the skin cancer dataset. It should be noted that the skin cancer dataset is binary, with two categories: benign and malignant. Table VII highlights the performance of deep learning models. The models were evaluated based on their accuracy, loss, precision, recall, specificity, and ROC values. According to Table VII, the CNN obtained the highest accuracy score of 90.30%, followed by the CapsNet with a value of 87.90%, and the GCN with a value of 86.60%.

TABLE VII. PERFORMANCE EVALUATION OF THE EEP LEARNING MODELS

Model	Accuracy	Loss	Precision	Recall	Specificity	ROC score
CNN	0.9030	0.3308	0.4953	0.5240	0.4660	0.5019
CapsNet	0.8790	0.0199	0.4820	0.5100	0.4520	0.4841
GCN	0.8680	0.0001	0.5000	0.4920	0.5080	0.4886

Furthermore, in terms of precision scores, the GCN surpassed the CNN and CapsNet, with 0.5000 vs 0.4953 and 0.4820 for the CNN and CapsNet, respectively. It should be noted that the GCN also had the lowest loss score of 0.0001, whereas the CNN and CapsNet had 0.3308 and 0.0199, respectively. As can be observed, all of the models attained a significant value in loss score, minimizing this loss in all situations and boosting the models' capacity to produce accurate predictions. In this study, the CapsNet model performed second best in terms of accuracy, producing significant results in recall (0.5100) compared to the GCN model's score of 0.4920. The recall values of the models show that there is potential for improvement, but their significance is contextual. They emphasize the models' capacity to recognize positive cases, and fine-tuning procedures may be used to increase this element, which is especially important when limiting false negatives.

Figs. 4–6 show the confusion matrices of the CNN, CapsNet, and GCN, respectively, to help understand the aforementioned results. These visual representations provide a brief and complete assessment of a model's categorization performance. The matrix categorizes predictions as TP, TN, FP, and FN, providing information about the models' accuracy, precision, recall, and overall efficacy. The confusion matrix analysis allows for a more detailed view of the model's strengths and limitations, directing additional development to improve its predictive skills and overall performance in classifying the skin cancer masses.

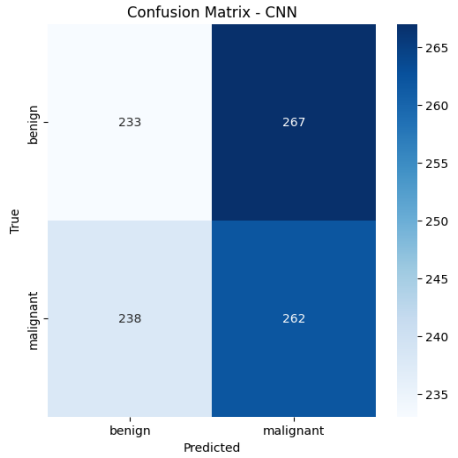

Fig. 4. Confusion matrix of the CNN model.

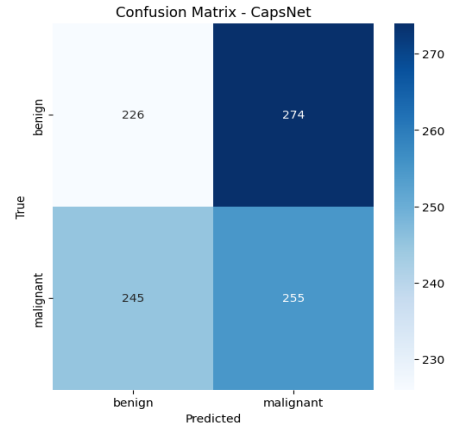

Fig. 5. Confusion matrix of the CapsNet model.

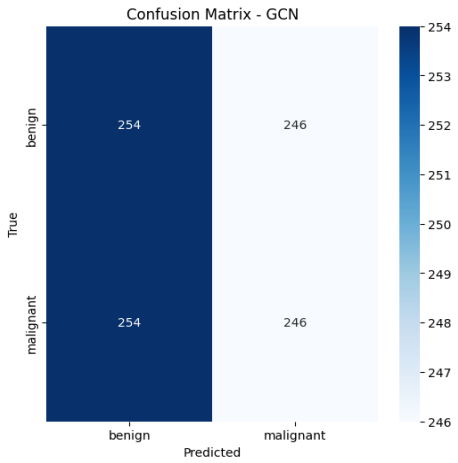

Fig. 6. Confusion matrix of the GCN model.

Fig. 7 also depicts the accuracies reached by the CNN, CapsNet, and GCN models in training the skin cancer data. In terms of accuracy, the CNN achieved 90.30%, followed

by CapsNet at 87.90% and the GCN at 86.60%. Among the deep learning models, CNN fared the best. The model accuracy results obtained by training the models demonstrate the superiority of the CNN in training skin cancer data, without undermining the performance of the CapsNet and GCN models. In terms of medical imaging prediction and analysis, CNN has shown to be more effective in many cases, and the findings of this study also highlight the capacity of CNN and DL models to train medical images in cases of data imbalance.

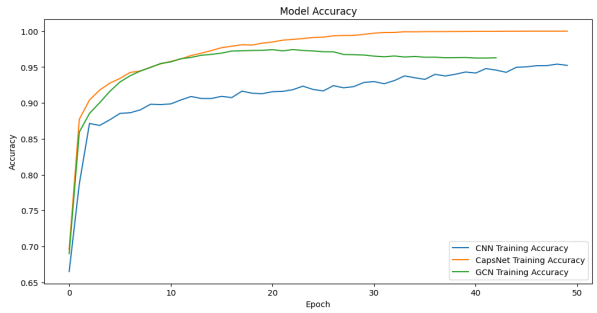

Fig. 7. Visual representation of the models' accuracy scores.

Furthermore, Fig. 8 also displays the loss values score of the DL models used in this study. The GCN had the lowest loss score of 0.001, followed by the CapsNet, which had a value of 0.199, and the CNN, which had a value of 0.3308. In general, lower model loss indicates higher performance in training processes. Monitoring the loss over time during training allowed us to determine whether the model is approaching an acceptable response. The models' decreasing loss after the epochs suggests that the models are learning and adjusting their weights to better suit the training skin cancer data.

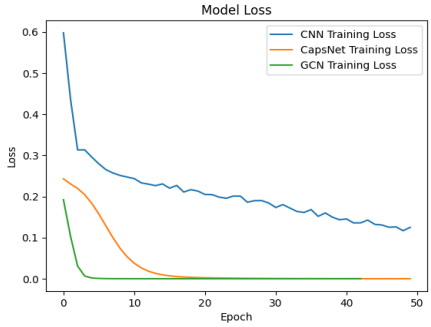

Fig. 8. Visual representation of the loss function of the models.

Furthermore, the Receiver Operating Characteristics (ROC) of the deep learning models were computed. The Receiver Operating Characteristics (ROC) scores are used to evaluate the efficacy of the models. A well-known deep learning assessment statistic is the ROC score. The ROC measures a classification model's ability to distinguish between skin cancer data across many classification criteria. Fig. 9 depicts the ROC scores of the models used in the present study. Albeit, many medical imaging collections in clinical settings suffer from an imbalance problem, which makes it difficult to spot outliers (rare health care occurrences), because most classification algorithms assume equal incidence of classes.

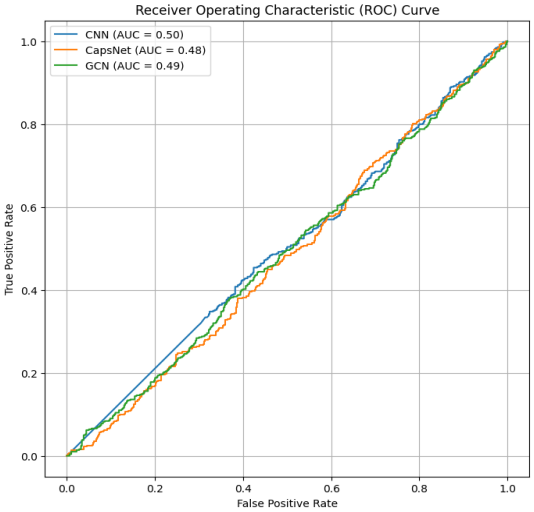

Fig. 9. The ROC curves of the models.

The ROC values of the models used in this study are slightly over 0.5 for this task, which involves infrequent occurrences or uneven class distributions; yet, they indicate that the model is suitably categorizing instances of the minority class, proving efficacy above random chance. This is especially important in sectors such as medical diagnostics, where the emphasis is on recognizing rare events. A comparable analysis conducted by Juan *et al.* [13] and Zhen *et al.* [30] in the study of breast lesion and liver tumor yielded lower ROC values than the current study. The models' results suggest that their capacity to recognize these infrequent occurrences, even with a ROC slightly over 0.5, adds useful information, underlining the need of context-specific judgments.

3) Summary of the deep learning models: CNNs are commonly employed in deep learning for image identification applications, employing convolutional layers to identify hierarchical features. They frequently attain great accuracy, as this study demonstrates to the literature with an accuracy of 90.30%, making them useful for a variety of computer vision applications. Furthermore, Capsule Neural Networks (CapsNet) strive to circumvent some limitations of CNNs by more efficiently capturing hierarchical spatial connections. While CapsNet shows potential, their accuracy, precision, recall, specificity, and ROC curves might differ depending on the job and dataset. The CapsNet obtained 87.90% accuracy in this study, supporting the conclusion above. CapsNet are particularly appealing for image challenges involving part-whole interactions. Gabor Capsule Networks (GCN) include Gabor filters into the capsule structure, allowing the model to extract complex patterns and textures. Gabor Capsule Networks' performance metrics are determined by the interaction of capsule routing techniques and Gabor filter responses, with possible advantages in collecting finer features when compared to regular CapsNet. The GCN attained 86.80% accuracy in this study, which is

significant. CNN performs well in a variety of visual recognition tasks, but CapsNet, including Gabor Capsule Networks, explores unique techniques to increase feature learning. Each model's performance is task-dependent, and their evaluation includes taking into account accuracy, precision, recall, specificity, and ROC curves to acquire a full knowledge of their strengths and limits in various applications. Fig. 10 summarizes all of the assessment criteria used to examine the deep learning models employed in this study.

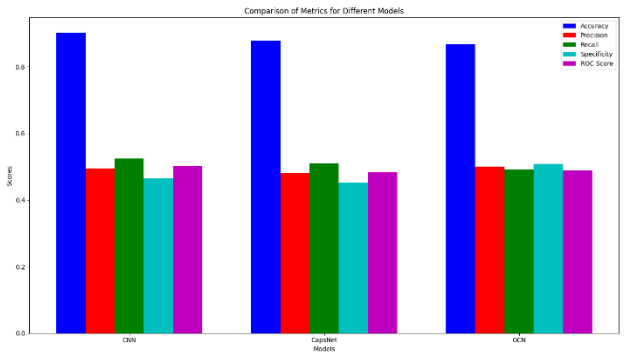

Fig. 10. Summary of the performance evaluation of the deep learning models.

IV. Discussion

Skin cancer is the abnormal growth of skin cells that most typically affects sun-exposed skin. This common kind of cancer, however, can develop on areas of the skin that are rarely exposed to sunlight. The three most frequent types of skin cancers are basal cell carcinoma, squamous cell carcinoma, and melanoma. Melanoma is the most severe type of skin cancer. This study used melanoma skin cancer data that was cleaned using multiple data preprocessing approaches so that the deep learning models could understand it. The categorization of skin cancer has improved with the advancement of technology. Because early identification and treatment of skin cancer can reduce its impact, this study used deep neural network models such as convolutional neural network, capsule neural network, and Gabor capsule network. The outputs of the methods used in this study gave significant empirical results in the realm of skin cancer categorization. The innovative technique and original analysis of deep learning models were assessed using a variety of performance metrics indicators. The convolutional neural network obtained 90.30% accuracy, the capsule neural network reached 87.9% accuracy, and the Gabor capsule network achieved 86.80% accuracy. The Gabor capsule network obtained the lowest loss score of 0.001, followed by the capsule neural network at 0.199 and the convolutional neural network at 0.3308. In general, lesser model loss suggests better training process effectiveness. We were able to detect whether the model is approaching an acceptable answer by tracking the loss over time throughout training. The diminishing loss of the models after the epochs implies that the models are learning and modifying their weights to better fit the training skin cancer data. This study has helped healthcare practitioners and stakeholders reduce and treat the effect of skin cancer based on melanoma lesions. The results are related to the state-of-the-art in the field of research, demonstrating that our models outperformed their results. Table VIII summarizes the proposed approach in comparison to previous research.

TABLE VIII. Comparison of The Results with Other Studies

Research	Dataset type	Model employed	Accuracy (%)
Riyadh *et al.* [15]	Melanoma skin	CNN	89.50
Saeed and Teemu [31]	Melanoma skin	Ensemble CNN	87.00
Fawzy *et al.* [14]	Melanoma skin	CNN	-
Tahir *et al.* [32]	Melanoma skin	CNN	89.68
Ajel *et al.* [33]	Melanoma skin	CNN	86.29
Proposed model	Melanoma skin	CNN, CapsNet, GCN	90.30, 87.90, 86.80

According to Table VIII, the proposed models outperformed the prior research in terms of accuracies. Furthermore, the majority of the models used CNN architectures without considering other standalone deep learning models. For instance, Riyadh *et al.* [15] considered only the CNN architectures of DenseNet201 and MobileNetV2 in its configuration. Additionally, in the study by Ajel *et al.* [33], the authors employed only the ResNet-50 architecture of the CNN to configure their model. It must be emphasized that, CapsNet use capsules and dynamic routing to preserve feature hierarchies, whereas standard CNNs may lose this information owing to pooling. GCN expand on this by including Gabor filters for better edge detection and texture representation, simulating human visual perception [27]. CapsNet and GCN outperform standard CNNs in terms of transformation robustness and feature extraction sophistication. Both configurations of the CapsNet and GCN improve transformation robustness and spatial information preservation over conventional pooling techniques in CNN as employed by the state-of-the-art. The CapsNet and GCN architectures are used in the current study, and the researchers believe they are a valuable addition and innovation in the domain of DL models for medical imaging analysis and detection because they preserve spatial hierarchies while improving feature extraction and providing superior transformation robustness.

V. Conclusion

Melanoma incidence has steadily increased over the previous few decades and is predicted to continue rising internationally. Melanoma characteristics are surprising and determined by factors such as age, gender, race, and location. DL models are used in this article to describe the development of a computationally demanding strategy based on the use of melanoma skin cancer data. The dataset comprises images of varying resolutions, and it is also incredibly unbalanced, which is a common difficulty in medical imaging and may impact the final findings. Convolutional neural network, capsule neural network, and Gabor capsule network are the models employed. The models correctly distinguished between melanoma and

noncancerous instances. Several performance evaluation indicators are used to enhance the models' performance. The results of the models indicate that the convolutional neural network is superior with an accuracy of 90.30%, followed by the capsule neural network with 87.90% and the Gabor capsule network with 86.80% in accuracies. To further evaluate the models' performance, the loss scores obtained by the models are significant, with lower scores obtained by all models. The Gabor capsule network obtained the lowest loss score of 0.001, followed by the capsule neural network at 0.199 and the convolutional neural network at 0.3308. The proposed models outperformed existing deep learning-based strategies in terms of score, making it a potential strategy for skin cancer diagnosis, particularly on unbalanced datasets. Our findings contribute to the evidence that deep learning techniques are helpful in dermatology and other sectors of medicine.

The results acquired by the models, like any empirical study, are prone to different biases, most notably data set imbalance, which is a prevalent difficulty in medical imaging. This is clarified such that the conclusions cannot be immediately applied to other datasets that have been trained using various approaches. To confirm the results, more study and experimentation on other high-quality, properly curated data sets are required. While we aimed to prevent overfitting by employing well-planned training, validation, and testing criteria, as well as carefully selected performance assessment measures, architectural optimization and hyperparameter tweaking. Architectural optimization and hyperparameter tuning are critical in deep learning to handle reproducibility issues and avoid overfitting. We can build more stable and generalizable models by carefully changing network design and fine-tuning hyperparameters including learning rates, batch sizes, and regularization approaches. These methods serve to ensure that models function consistently across diverse datasets and experimental setups, increasing their reliability and practical application in real-world situations. The situation is exacerbated by the blurring of the border between techniques and data preparation, particularly in deep learning, making meaningful head-to-head comparisons difficult. To improve the performance of the models, the experimental setup used in this study can be expanded in terms of creating baseline and benchmark approaches. Although the study uses skin cancer data to classify melanoma lesions, the technique may be further enhanced by using generic combinations of various deep learning architectures.

Conflict of Interest

The authors declare no conflict of interest.

Author Contributions

SA had the conceptualization, and performed the methodology, software, writing—original draft preparation, writing—review and editing, data curation; VV also had the conceptualization, and performed the validation, resources, writing—review and editing, supervision, project administration; TZ also had the conceptualization, and performed validation, resources, writing—review and editing, supervision, project administration; PA also had the conceptualization, and performed the validation, resources, writing—review and editing, supervision; DG performed data curation, software, writing—review and editing; methodology; RMOMG did the writing—review and editing, methodology. All authors had approved the final version.

Acknowledgment

The authors are grateful to Malcolm Afrifa and Adwoa Afriyie, popularly known as Amanpene, for their encouragement and advise throughout the study.

References

[1] A. Gharawi, M. D. Alahmadi, and L. Ramaswamy, "Self-supervised skin lesion segmentation: An annotation-free approach," *Mathematics*, vol. 11, no. 18, pp. 1–14, 2023.

[2] A. Shamsi *et al.*, "A novel uncertainty-aware deep learning technique with an application on skin cancer diagnosis," *Neural Comput. Appl.*, vol. 35, no. 30, pp. 22179–22188, 2023.

[3] S. Hao *et al.*, "GSCEU-Net: An end-to-end lightweight skin lesion segmentation model with feature fusion based on U-Net enhancements," *Inf.*, vol. 14, no. 9, 2023.

[4] S. Bibi *et al.*, "MSRNet: Multiclass skin lesion recognition using additional residual block based fine-tuned deep models information fusion and best feature selection," *Diagnostics*, vol. 13, no. 19, pp. 1–22, 2023.

[5] WHO.int. (2023). Radiation: Ultraviolet (UV) radiation and skin cancer. [Online]. Available: https://www.who.int/news-room/questions-and-answers/item/radiation-ultraviolet-(uv)-radiation-and-skin-cancer?gclid=CjwKCAiA98WrBhAYEiwA2WvhOq9YPRwuuwn0M7w1JlVajiYhQu8wsN9DOWxQxvc2gx4iBntGTSFRwxoCJ4MQAvD_BwE#

[6] Skincancer.org. (2023). More than moles: When melanoma doesn't look like you think it should—The skin cancer foundation. [Online]. Available: https://www.skincancer.org/blog/more-than-moles-melanoma/

[7] A. M. G. Alnooj, M. Ghobadi, M. Mousavi-Khattat, D. Zohrabi, M. Sekhavati, and A. Zarrabi, "Cytotoxicity of curcumin-loaded magnetic nanoparticles against normal and cancer cells as a breast cancer drug delivery system," *Nanofabrication*, vol. 7, pp. 1–16, 2022.

[8] K. Shen *et al.*, "Prediction of survival and immunotherapy response by the combined classifier of G protein-coupled receptors and tumor microenvironment in melanoma," *Eur. J. Med. Res.*, vol. 28, no. 1, pp. 1–16, 2023.

[9] Y. Zhao *et al.*, "Leveraging a disulfidptosis-related signature to predict the prognosis and immunotherapy effectiveness of cutaneous melanoma based on machine learning," *Mol. Med.*, vol. 29, no. 1, 2023.

[10] B. Flora *et al.*, "Recent updates on metal-polymer nanocomposites in 3D bioprinting for tissue engineering applications," *Nanofabrication*, vol. 8, pp. 9–11, 2023.

[11] F. Grignaffini *et al.*, "Anomaly detection for skin lesion images using convolutional neural network and injection of handcrafted features: A method that bypasses the preprocessing of dermoscopic images," *Algorithms*, vol. 16, no. 10, 2023.

[12] L. Ichim, R. I. Mitrica, M. O. Serghei, and D. Popescu, "Detection of malignant skin lesions based on decision fusion of ensembles of neural networks," *Cancers (Basel).*, vol. 15, no. 20, 2023.

[13] C. K. Juan *et al.*, "Deep convolutional neural network with fusion strategy for skin cancer recognition: Model development and validation," *Sci. Rep.*, vol. 13, no. 1, pp. 1–9, 2023.

[14] S. Fawzy, H. El-Din Moustafa, E. H. AbdelHay, and M. M. Ata, "A deep convolutional structure-based approach for accurate recognition of skin lesions in dermoscopy images," *Int. J. Electr. Comput. Eng.*, vol. 13, no. 5, pp. 5792–5803, 2023.

[15] S. Riyadh, S. Mohammed, and M. S. Mohd, "Melanoma skin cancer classification based on CNN deep learning algorithms," *Malaysian J. Fundam. Appl. Sci.*, vol. 19, pp. 299–305, 2023.
[16] J. A. Onesimu, V. U. Nair, M. K. Sagayam, J. Eunice, M. H. A. Wahab, and N. Sudin, "SkCanNet: A deep learning based skin cancer classification approach," *Ann. Emerg. Technol. Comput.*, vol. 7, no. 4, pp. 35–45, 2023.
[17] Api.isic-archive.com. (2023). ISIC Archive. [Online]. Available: https://api.isic-archive.com/collections/294/
[18] S. Afrifa, V. Varadarajan, P. Appiahene, and T. Zhang, "A novel artificial intelligence techniques for women breast cancer classification using ultrasound images," *Clin. Exp. Obstet. Gynecol.*, vol. 50, no. 12, 2023.
[19] S. Bechelli and J. Delhommelle, "Machine learning and deep learning algorithms for skin cancer classification from dermoscopic images," *Bioengineering*, vol. 9, no. 3, pp. 1–18, 2022.
[20] R. O. Ogundokun *et al.*, "Enhancing Skin cancer detection and classification in dermoscopic images through concatenated MobileNetV2 and Xception models," *Bioengineering*, vol. 10, no. 8, 2023.
[21] S. Afrifa, T. Zhang, X. Zhao, P. Appiahene, and M. S. Yaw, "Climate change impact assessment on groundwater level changes: A study of hybrid model techniques," *IET Signal Process.*, vol. 17, e12227, 2023.
[22] F. Brutti *et al.*, "Artificial intelligence algorithms for benign vs. malignant dermoscopic skin lesion image classification," *Bioengineering*, vol. 10, no. 11, 1322, 2023.
[23] S. Afrifa, V. Varadarajan, P. Appiahene, T. Zhang, and E. A. Domfeh, "Ensemble machine learning techniques for accurate and efficient detection of botnet attacks in connected computers," *MDPI Eng*, pp. 650–664, 2023.
[24] M. Azeem *et al.*, "Neural networks for the detection of COVID-19 and other diseases: Prospects and challenges," *Bioengineering*, vol. 10, no. 7, pp. 1–28, 2023.
[25] Y. Shang, N. Xu, Z. Jin, and X. Yao, "Optimization of the routing of capsule network based on multiscale information and self-attention mechanism," *J. Electron. Imaging*, vol. 31, no. 2, pp. 1–13, 2022.
[26] S. Toraman, T. B. Alakus, and I. Turkoglu, "Convolutional capsnet: A novel artificial neural network approach to detect COVID-19 disease from X-ray images using capsule networks," *Chaos, Solitons and Fractals*, vol. 140, 2020.
[27] A. H. Khalifa, N. A. Zaher, A. S. Abdallah, and M. W. Fakhr, "Convolutional neural network based on diverse gabor filters for deepfake recognition," *IEEE Access*, vol. 10, pp. 22678–22686, 2022.
[28] S. Afrifa and V. Varadarajan, "Cyberbullying detection on Twitter using natural language processing and machine learning techniques," *Int. J. Innov. Technol. Interdiscip. Sci.*, vol. 5, no. 4, pp. 1069–1080, 2022.
[29] W. K. Adu, P. Appiahene, and S. Afrifa, "VAR, ARIMAX and ARIMA models for nowcasting unemployment rate in Ghana using Google trends," *J. Electr. Syst. Inf. Technol.*, pp. 1–16, 2023.
[30] S. H. Zhen *et al.*, "Deep learning for accurate diagnosis of liver tumor based on magnetic resonance imaging and clinical data," *Front. Oncol.*, vol. 10, no. May, pp. 1–14, 2020.
[31] A. Saeed and Q. Teemu, "Transfer learning with ensembles of deep neural networks for skin cancer detection in imbalanced data sets," *Neural Process. Lett.*, vol. 55, no. 4, pp. 4461–4479, 2023.
[32] M. Tahir, A. Naeem, H. Malik, J. Tanveer, R. A. Naqvi, and S. Lee, "DSCC_Net: Multi-classification deep learning models for diagnosing of skin cancer using dermoscopic images," *MDPI Cancers*, 2023.
[33] A. R. Ajel, A. Q. Al-Dujaili, Z. G. Hadi, and A. J. Humaidi, "Skin cancer classifier based on convolution residual neural network," *Int. J. Electr. Comput. Eng.*, vol. 13, no. 6, pp. 6240–6248, 2023.